Journal of Food Engineering 371 (2024) 111967

Contents lists available at ScienceDirect

Journal of Food Engineering

journal homepage: www.elsevier.com/locate/jfoodeng

Using ice surrounding to improve radio frequency tempering uniformity of bulk pacific white shrimp (*Litopenaeus vannamei*)

Yajin Zhang [a,b,c,d], Xiangqing Chen [a,b,c], Yu Liu [a,b,c], Feng Li [a,b,c], Juming Tang [e], Hu Shi [a,b,c], Yang Jiao [a,b,c,*]

[a] College of Food Science and Technology, Shanghai Ocean University, Shanghai, 201306, China
[b] Engineering Research Center of Food Thermal-Processing Technology, Shanghai Ocean University, Shanghai, 201306, China
[c] National R&D Branch Center for Freshwater Aquatic Products Processing Technology (Shanghai), Shanghai, 201306, China
[d] College of Food Science and Technology, Huazhong Agricultural University, Wuhan, Hubei Province, 430070, China
[e] Department of Biosystems Engineering, Washington State University, Pullman, WA, 99164-6120, USA

ARTICLE INFO

Keywords:
Crushed ice
Porosity
Tempering uniformity

ABSTRACT

Localized heating is prone to occur in foods with irregular geometries subjected to radio frequency (RF) heating. Adding surrounding medium may effectively improve the heating uniformity of food with irregular shape like shrimps. A computer simulation model was constructed and verified by experiments to explore the RF tempering uniformity of bulk pacific white shrimps (*Litopenaeus vannamei*) surrounded by loosely stacked crushed ice (LSCI, porosity $\varphi = 0.62$), compacted crushed ice (CCI, $\varphi = 0.44$), and ice block (IB, $\varphi = 0$), respectively. Thermal and dielectric properties of shrimp cephalon, tail and caudal fan were obtained respectively, and assigned to the according portions of the geometrical model. Results showed that the caudal fan of shrimp was over-heated (48.8 °C) when the body temperature reaching around −2.0 °C without surrounding medium. Comparatively, only a 7.8 °C difference was found between the hot and cold spots in shrimps surrounded by CCI. Results indicated surrounding ice with reduced porosity significantly improved RF tempering uniformity of bulk frozen shrimps.

1. Introduction

Litopenaeus vannamei, commonly known as Pacific white shrimp, represents one of the most prevalent commercial shrimp species on a global scale (Li et al., 2022). Freezing serves as a widely utilized preservation method for shrimp, effectively deterring spoilage and impeding melanosis induced by polyphenol oxidase activation. Typically, frozen shrimp necessitate tempering before undergoing cutting or further processing. In contrast to thawing and defrosting, tempering involves elevating the temperature of frozen foods to around −4 to −1 °C, enabling easy cutting without significant quality deterioration. The industry commonly employs water and cold-room tempering, but cold-room tempering typically necessitates a longer time, which may accelerate protein oxidation and increase microbial loads. Meanwhile, water tempering may remove water-soluble nutrients and generate a substantial amount of wastewater. Developing novel tempering methods with higher efficiency and better control is crucial to prevent food quality degradation and nutritional loss.

Several novel tempering technologies have been explored in food industry, including ohmic (Chen et al., 2022; Liu et al., 2017), ultrasonic (Cai et al., 2019; Guo et al., 2021), high voltage electrostatic fields (Tang et al., 2017), microwave (Watanabe and Ando, 2021), and radio frequency (Zhang, et al., 2021a) technologies. Among all, radio frequency (RF) technology with its characteristics of fast and volumetric heating, higher penetration depth, and non-contact heating has been recognized as a suitable technology for frozen food tempering. However, non-uniform heating is still one of the major problems hinders its wide application in food industry. In recent years, several studies have investigated the relationship between the surrounding medium and dielectric properties of the food for the improvement of RF heating uniformity. It was found that the non-uniform heating was caused by the significant difference of dielectric properties between food and its surrounding medium (usually air) (Jiao et al., 2014). Thus, addition of surrounding medium with similar dielectric properties as the food would balance the non-uniform heating and generate a uniform electric field distribution within the food material. Some researchers found RF

* Corresponding author. College of Food Science and Technology, Shanghai Ocean University, Shanghai, 201306, China.
E-mail address: yjiao@shou.edu.cn (Y. Jiao).

https://doi.org/10.1016/j.jfoodeng.2024.111967
Received 26 May 2023; Received in revised form 2 January 2024; Accepted 14 January 2024
Available online 19 January 2024

heating uniformity was improved by immersing food into surrounding medium with similar dielectric constant and lower dielectric loss factor to the food itself (Birla et al., 2008). Li et al. (2021) found that 70% glycerol solution as a liquid surrounding medium can effectively reduce the edges overheating for RF tempering frozen beef. Zhang et al. (2021b) also showed that crushed ice, as a particulate surrounding medium, exhibited a positive influence on improving the RF tempering uniformity of six layers of shrimps. However, the porosity of crushed ice may vary due to its porous structure and various particle size. Several research focused on the effect of porosity of the bed in bulk material subjected to RF heating, e.g., walnut (Zuo et al., 2022), wheat kernels (Jiao et al., 2015) and black pepper (Liu et al., 2023) on the heating uniformity. Zuo et al. (2022) found that a better overall RF heating uniformity was obtained with lower porosity or small particle size of walnut kernels in a rectangular container. Wang et al. (2024) also reported that lower porosity improved heating uniformity of cauliflowers. These studies demonstrated that bed porosity has a significant impact on the distribution of bulk temperature within the kernel. This observation may prompt further investigation into how the porosity of the particulate surrounding medium influences the heating behavior of the enclosed sample. Ice is convenient to obtain and has similar dielectric properties as most of the frozen foods with high water content, which would hypothetically enhance the food tempering uniformity. However, a whole piece of ice surrounding would result in an unbreakable shell for the tempered product. Instead, crushed ice with similar properties as whole piece of ice can be easily stuffed into containers to surround foods and removed when necessary. Thus, crushed ice was identified as the target surrounding medium and studied for further possible application in this study.

Computer simulation is an advanced tool for efficiently predicting the volumetric electromagnetic field and temperature distribution in calculated domains that are difficult to attain in experiments. Some researchers have developed computer models with COMSOL Multiphysics software to predict the heating uniformity improvement by inserting polypropylene or aluminum plates into watermelon seeds (Guan et al., 2022) or adding high-dielectric-constant material around the wheat flour (Miran and Palazoglu, 2023). Thus, it is reasonable to utilize finite element method (FEM) to evaluate the effect of surrounding medium characteristics on RF tempering uniformity and predict the electric field distribution in irregular-shape aquatic product.

This study aimed to address the knowledge gap regarding the unclear impact of the porosity of the particulate surrounding medium on the uniformity of heating in bulk frozen shrimps during RF tempering. Thus, the objectives of the current study are to investigate the effect of dielectric and thermophysical properties of different parts of shrimp on the uniformity of RF tempering, and to reveal the influence of surrounding ice porosity on RF tempering uniformity of shrimps with both FEM modeling and experimental methods.

2. Materials and methods

2.1. Pacific white shrimp sample preparation

Pacific white shrimps were purchased from a local aquatic product market (Luchaogang, Shanghai, China), and transported with oxygen to the laboratory alive. After arrival, shrimps with similar sizes were selected for experiment and geometrical modeling. Each individual shrimp was wiped with absorbent paper, and every 6 of them were placed in a zip-lock bag as a group. All shrimps in bags were stored in a -20 ± 2 °C freezer (BCD-610 W, SIMENS, Germany) until death for 48 h before experiments.

The moisture content of different sections of shrimp was measured by the following method. Each prepared homogenates of cephalon, tail, and caudal fan were weighted (5.0 ± 0.5 g) and then dehydrated to a constant weight at 105 °C with a constant temperature oven, respectively, for moisture content determination. The experiment was repeated three times, and the moisture content of materials is calculated with the following equation:

$$MC = \frac{(M_0 - M_1)}{M_0} \times 100\% \quad (1)$$

where M_0 and M_1 are the weight of the sample (g) before and after being dehydrated, respectively.

2.2. Mathematical description

2.2.1. Model assumptions

The following assumptions were proposed to simplify the calculation of RF tempering process: 1) The shrimp legs, the shell of tail and cephalon were neglected in geometrical modeling since they were too thin to be successfully meshed for obtaining a valid solution. 2) The melting of crushed ice during tempering was not considered in simulation since although the ice pieces melted slightly in RF tempering process, it had an insignificant effect on RF tempering uniformity of the food samples according to a previous study (Zhang et al., 2021b). 3) The container of shrimp was neglected in modeling since the effect of the polypropylene container on RF tempering uniformity was considered minimal based on a previous study (Zhang et al., 2021b). 4) Identical shrimp geometry and size were assumed for shrimp samples in simulation since shrimps with similar sizes were selected for RF tempering experiments to ensure the consistency of experiment.

2.2.2. Physical model

The physical model of shrimp tempered in RF was built based on a commercial 12 kW 50 Ω RF heater (Labotron 12, SAIREM Decines Charpeu, France). The generation and transmission of RF wave were simplified to the voltage value assigned to the top electrode as the energy source (Li et al., 2018). The shrimp geometry was depicted with Autodesk 3D MAX software (Fig. 1). The shells of cephalon, shells of tails and the shrimp legs were neglected to simplify the modeling process. The layout of shrimps was shown in Fig. 1(b). A 0.3 cm gap was created between adjacent shrimps in the same layer to account for the presence of shrimp legs. Also, a layer of ice (1 cm thick) was filled in between each layer of shrimps for better surrounding.

2.2.3. Governing equations

Maxwell's equations described the relationship between electromagnetic field and electric current. However, obtaining the solution of Maxwell's equations was complex and time-consuming. Researchers have utilized Laplace's equation with quasi-static hypothesis and effectively applied to RF heating process simulation (Marra et al., 2007). Laplace's equation is expressed as follows:

$$-\nabla \bullet ((\sigma + j2\pi\varepsilon_0\varepsilon^{'})\nabla V) = 0 \quad (2)$$

where σ is the electrical conductivity of the food material (S m^{-1}), $j = \sqrt{-1}$, ε_0 is permittivity of electromagnetic wave in free space (8.854×10^{-12} F m^{-1}), $\varepsilon^{'}$ is the dielectric constant of food material, and V is the electric potential across the electrode gap (V). The amount of electromagnetic power convert to heat is given by:

$$P = 2\pi f \varepsilon_0 \varepsilon^{''} |\overrightarrow{E}|^2 \quad (3)$$

where P is the electromagnetic power conversion in food per unit volume (W m^{-3}), f is the working frequency of RF equipment (Hz), $\varepsilon^{''}$ is the loss factor of food materials, and $\overrightarrow{E}$ is the electric field intensity in food material (V m^{-1}).

The temperature change in food due to the conversion of electromagnetic energy to heat and the heat transfer between the food and atmosphere, which is described by the following equation:

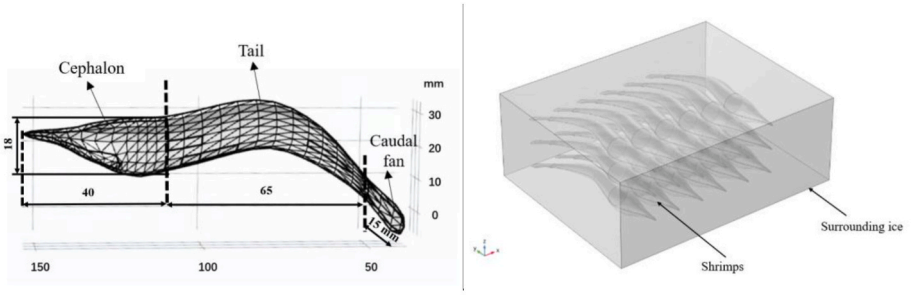

Fig. 1. Physical model (a) and arrangement (b) of shrimp for simulation (unit: mm).

$$\rho_b c_p \frac{\partial T}{\partial t} = \nabla(k\nabla T) + P \tag{4}$$

where $\partial T/\partial t$ is the instant heating rate in food material (°C s^{-1}), k is the thermal conductivity (W m^{-1} K^{-1}), ρ_b is the bulk density (kg m^{-3}), and c_p is specific heat (kJ kg^{-1} K^{-1}) of the food material.

2.2.4. Initial and boundary conditions

Boundary conditions for the modeling process were described as follow:

– The top electrode of RF system (27.12 MHz) was the source of electromagnetic energy. Since the voltage of the top electrode was difficult to be measured accurately during RF tempering, an estimation equation (Eq. (5)) was applied to estimate the voltage of the top electrode based on an assumption of uniform electric field distribution in the food material (Jiao et al., 2015). For shrimp without surrounding medium, the dielectric and thermophysical properties of shrimp tail meat were used to calculate the electric potential. For shrimp surrounding by ice, the average of both dielectric and thermophysical properties of shrimp tail meat and ice were used to calculate the electric potential. After estimation, voltages of 2700 and 4000 V was used in the simulation of shrimp tempering without and with ice, respectively. Trial and error were then performed by adjusting the voltage until the predicted heating curve of sample matched the experimental results (Jiao et al., 2015; Tong et al., 2022).

$$V = \left(d_{air}\sqrt{(\varepsilon')^2 + (\varepsilon'')^2} + d_{mat}\right)\left(\sqrt{\frac{\rho c_p}{\pi f \varepsilon_0 \varepsilon''}\frac{dT}{dt}}\right) \tag{5}$$

where d_{air} is the distance from the top electrode to the top surface of sample (m), d_{mat} is the height of sample (m).

– The metal shell of the RF cavity was set as electric insulation ($\nabla \vec{E} = 0$).
– The bottom plate was maintained grounded ($V = 0$).

Boundary and initial conditions for energy equation to determine the temperature distribution inside the sample load were.

– Convective heat transfer (the 3rd type of boundary condition) was considered through the external surfaces of the ice:

$$-k \bullet \nabla T = h \cdot (T - T_{\text{air}}) \tag{6}$$

where T is the temperature of ice surface (°C), and T_{air} is the temperature of the surrounding air (20 °C). The convective heat transfer coefficient (h) was estimated with the following equations (Singh and Heldman, 2001):

$$h = \frac{N_u \lambda}{L} \tag{7}$$

$$N_u = \mathrm{C}(GrPr)^n \tag{8}$$

$$Gr = \frac{\beta g \Delta T L^3 \rho^2}{\mu^2} \tag{9}$$

where Nu is the Nusselt number, 75.60; ρ is the density of air at 20 °C, 1.205 (kg m^{-3}); λ is the thermal conductivity of air, 0.02591 (W m^{-1} K^{-1}); Pr is the Prandtl number, 0.686; Gr is the Grashof number, 5.67×10^8; μ is the dynamic viscosity of the air at 20 °C, 1.81×10^{-5} (Pa s^{-1}); β is the reciprocal of temperature (1/T), K^{-1}; g is the gravitational acceleration, 9.8 (m s^{-2}); L is the sample length, 0.19 (m); ΔT is temperature difference between sample center and air (K); and C (0.53), n (0.25) are constant. The estimated convective heat transfer coefficient is 10.31 (W m^{-2} K^{-1}), which was applied as the boundary condition between sample/ice and air in this study.

– For initial conditions, the shrimps and crushed ice were assumed to be at a uniform constant temperature of −20 °C and 0 °C, respectively, which was corresponding with the experimental condition. However, the initial temperature of IB (with a porosity of 0) was set as −20 °C since water and shrimps were frozen together until the temperature of both reached −20 °C in experiment.

The initial and boundary conditions were summarized in Table 1.

2.3. Model parameters

2.3.1. Dielectric and thermophysical properties of ice and shrimp tail, caudal fan, and cephalon

Each single shrimp was separated into three parts as cephalon, tail and caudal fan for properties determination. The cephalon was shelled and homogenized with a homogenizer (FJ200-SH, Biaoben Shanghai, China) for 1 min, and the tail (shelled) and caudal fan were minced with a grinder (JYL-C19V, Joyoung, Jinan, China) for 2 min, respectively.

The dielectric properties of ice and all three parts of shrimps were measured respectively within the frequency range of 20~100 MHz using an open-ended probe (Agilent N1501A, Agilent Technologies Inc., California, USA) connected to a network analyzer (Agilent E5071C, Agilent Technologies Inc., California, USA). Before measurements, the

Table 1
Initial and boundary conditions of the model.

Parameters	Values
Initial temperature of shrimps	−20 [°C]
Initial temperature of the crushed ice	0 [°C]
Initial temperature of a block of ice ($\varphi = 0$)	−20 [°C]
Air temperature	20 [°C]
Convective heat transfer coefficient	10.31 [W m^{-2} K^{-1}]
Working frequency	27.12 [MHz]
Electrode voltage	2700~4000 [V]
Electric insulation	0 [V]

equipment was calibrated in a mode for measuring the properties of air, the short-circuit block and deionized water at 25 °C. A customized sample holder (d = 2.5 cm, h = 10 cm) equipped with a type-K thermocouple wire (OMEGA Engineering, Norwalk, USA) was connected to an oil bath (Poly Science Products, Niles, USA) for properties measurement over a temperature range of −20 to 30 °C at 5 °C intervals. For different parts of shrimps, prepared homogenate was stuffed into the sample holder respectively, and the measuring probe was gradually lowered to fully contact the sample surface. A clamp was applied to clutch the probe and sample holder to avoid movement during measurement. Temperature was lowered from 30 to −20 °C for data collection. The detailed measurement system and procedures of experiments were described in Chen et al. (2021). To determine the dielectric properties of ice, room temperature tap water was filled into the custom-built sample holder and the measuring probe was kept immersed in liquid. Water was not filled full to avoid volume expansion and damage of probe. The temperature controlling system was set to −20 °C with the oil bath circulation system to gradually lower the water temperature, and the dielectric properties of the ice was determined from high to low temperature. All measurements were repeated three times.

The thermal conductivity of the shrimp was determined with a probe line heat source method (KD2-pro Decagon, Pullman, USA). The three parts homogenates of shrimps were stuffed in the self-made polyethylene container with a radius of 6 cm, respectively, and kept frozen in a freezer (BCD-610 W, SIMENS, Germany) at −20 °C for 24 h. Before freezing, a measuring probe was inserted into the sample center in order to accurately measure the thermal conductivity of the sample at −20 °C. The thermal conductivity of the each section of the shrimp was determined within the range of −20~30 °C in a step of 1 °C. The thermal conductivity of ice was adapted from a literature (Mohos, 2010).

The specific heat of shrimp was determined with a differential scanning calorimeter (DSC) method. Fifteen (15 ± 0.06) mg of each component was added to an aluminum pan (30 μL), hermetically closed with a lid, and placed in the DSC furnace (Q2000, TA Instruments, New Castle, USA). The measurement started with 1 min equilibration at −20 °C, followed by heating to 30 °C at 1 °C/min. The experiment was repeated three times. The specific heat of ice was adapted from the literature (Mohos, 2010).

The phase change was considered in the modeling with the measured apparent specific heat capacity, thermal conductivity and dielectric properties covering the phase transition temperature. Particularly, apparent specific heat capacity was used in modeling which considered the latent heat contribution during phase change. The measured properties of three parts of shrimp were assigned to the corresponding sections accordingly for modeling the whole tempering process. However, mass transfer due to melting (e.g. ice melted to water and water flowed due to gravity) was not considered in this study since water drip was barely observed from the RF tempering experiment.

2.3.2. Density of crushed ice and shrimp tail, caudal fan, and cephalon

The bulk density of crushed ice was determined by measuring the mass and bulk volume of samples. Crushed ice was prepared from tap water in an ice maker (XB-30 Xinzhi, Ningbo China), which was filled into a polypropylene container (19 × 13.5 × 8 cm^3) at 4 °C until full. In the case of loosely stacked ice, the crushed ice was poured into the polypropylene container without any mechanical pressing. However, for compacted stacking, after filling the container, the crushed ice was promptly pressed by hand using a rigid polypropylene sheet to reduce the porosity. From preliminary experiments, the weight of ice was determined and controlled both before and after compressing, respectively, to ensure the consistency. The bulk volume of crushed ice in both loosely stacked mode and compacted stacking mode was considered as the volume of polypropylene container since ice was fully filled. The homogenate of each three parts was filled into a glass container (3 × 3 × 4 cm^3) and weighed. The bulk density of crushed ice and shrimp was calculated with the following equation:

$$\rho_b = \frac{m}{V} \tag{10}$$

where ρ_b is the bulk density of crushed ice and three parts of shrimp (kg m^{-3}), m is the mass of ice and three parts of shrimp (kg), V is bulk volume of the polypropylene container and glass container (m^{-3}).

2.3.3. Properties for the crushed ice

The porosity of crushed ice (φ) was calculated from the bulk density (ρ_b, kg m^{-3}) of two stacking modes and the true density of ice (ρ_{bi}, kg m^{-3}). The theoretical porosities for various stacking modes for crushed ice can be calculated as follow (Liu et al., 2009):

$$\varphi = 1 - \frac{\rho_b}{\rho_{bi}} \tag{11}$$

The dielectric properties and thermal conductivity of crushed ice were difficult to be measured by experiment due to the porous structure. Thus, mixture average equations were used to obtain a valid estimation. The temperature of crushed ice produced by ice maker is approximately at 0 °C. It was observed that crushed ice slightly melted after 900 s RF treatment, and a small portion of the crushed ice mixture and water in the bottom container with a temperature not exceeding 2 °C. Therefore, in this study, we utilized the dielectric properties of ice block measured at 0 °C to calculate the dielectric properties of crushed ice with different porosities.

The dielectric properties of crushed ice were estimated by Complex Refractive Index mixture equation (CRIME), which was further used in developing computer simulation model for RF tempering:

$$\varepsilon^{\frac{1}{2}} = v_1(\varepsilon_1)^{\frac{1}{2}} + v_2(\varepsilon_2)^{\frac{1}{2}} \tag{12}$$

where ε is the complex permittivity of the mixture, ε_1 is the complex permittivity of medium in which pieces of complex permittivity ε_2 are dispersed, and v_1, v_2 are the volume fraction of the respective components, and $v_1 + v_2 = 1$.

Thermal conductivity of the crushed ice with different porosities was calculated as follows (Huang et al., 2018):

$$k_e = k_p \left[\frac{1 - \varphi^{\frac{2}{3}}\left(1 - \left(\frac{k_a}{k_p}\right)\right)}{1 - \varphi^{\frac{2}{3}}\left(1 - \left(\frac{k_a}{k_p}\right)\right)\left(1 - \varphi^{\frac{2}{3}}\right)} \right] \tag{13}$$

where k_e is the thermal conductivity of air-ice mixture (W m^{-1} K^{-1}), k_p is the thermal conductivity of ice (W m^{-1} K^{-1}), k_a is the thermal conductivity of air (W m^{-1} K^{-1}).

2.4. Simulations

A finite element method (FEM) based software, COMSOL Multiphysics®, (COMSOL Multiphysics 4.2, Burlington, MA, USA) was used for visualizing electromagnetic field and volumetric temperature distribution. The joule heating module, which conjugates the electric current and heat transfer models, was selected to simulate the RF tempering processes. After selecting the module, the 3D model of RF heating cavity and container were established in COMSOL Multiphysics® software, the 3D geometry of shrimp drawn in 3dmax® software was imported, and the arrangement of shrimp in a container was shown in Fig. 2. Based on the shape of shrimp, the shrimp body was divided into three sections, including shrimp cephalon, tail and caudal fan by adding two work planes at the shrimp head and tail. The measured value of dielectric and thermophysical properties of three parts of shrimp were assigned to the sections accordingly, respectively (Table 2). The dielectric and thermophysical properties of the ice with various porosities were assigned to the rest of the container volume (Table 3). The meshing size for the ice, cephalon, tail and caudal fan of shrimp were selected as “fine” and the RF cavity was meshed with an ordinary mesh. The mesh elements in the

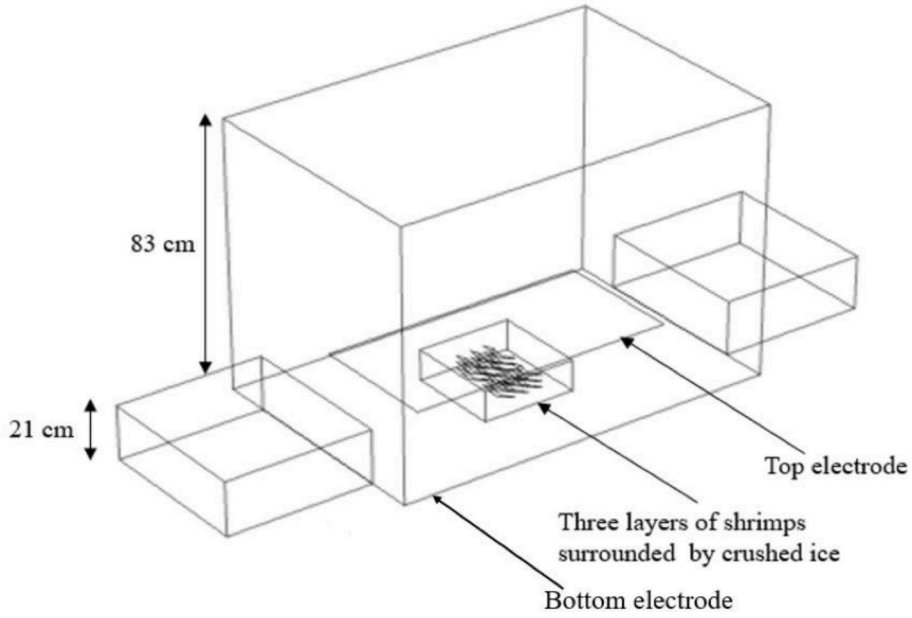

(a)

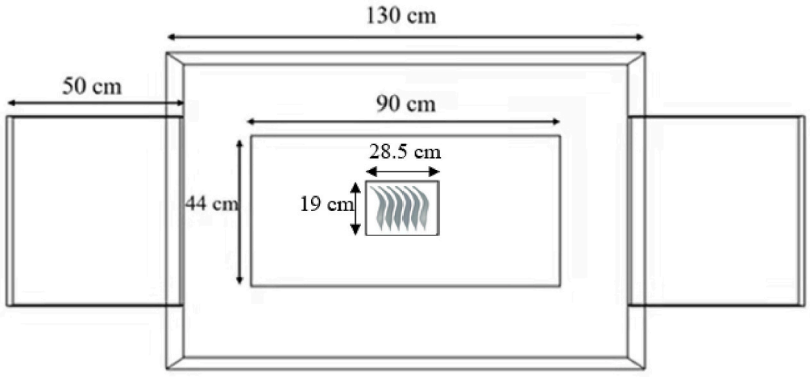

(b)

Fig. 2. Physical model of the RF cavity and food sample in RF tempering simulation including the system layout (a), and top view (b) with dimensions.

case of shrimps without ice consisted of 61,479 domain elements (tetrahedral), 7560 boundary elements (triangular), 1178 edge elements (linear), and 136 vertex elements. For shrimps with surrounding ice, the mesh elements consisted of 52,859 domain elements (tetrahedral), 8012 boundary elements (triangular), 1233 edge elements (linear), and 144 vertex elements. The mesh size was chosen based on the study of convergence when the difference of the maximum temperature between successive calculations was <0.1% (Li et al., 2018). Apparent heat capacity measured in *section 2.3.1* was used in modeling to take the phase change into consideration. The ice melting and fluid flow was neglected in this work since water drip was barely observed from the RF tempering experiment. The SPOOLES solver was selected with a time step of 0.01s, and the tempering time was set as 900 s with a step time of 0.1s. The simulation runs were conducted on a workstation with a Dell processor, dual Intel Xeon CPUs 2.60 GHz, 128 GB memory, and Windows Sever 2012 R2 Standard 64-bit operating system.

2.5. Tempering uniformity evaluation

The tempering uniformity of shrimps was evaluated using temperature uniformity index (*TUI*). The index describes the temperature deviation of each element from the volumetric average temperature as expressed (Li et al., 2018):

$$TUI = \frac{\int_0^{V_{vol}} |T - T_{av}| dV_{vol}}{(T_{av} - T_{\text{initial}}) V_{vol}} \tag{14}$$

where V_{vol} is the sample volume (m^3), T, T_{av}, and $T_{initial}$ are the transient, volumetric average and initial temperatures (°C) of the sample, respectively.

Table 2
Dielectric and thermophysical properties of shrimp used in computer simulation.

Parameters				Values								
Density				Cephalon 1.11 [kg m^{-3}]			Tail meat 1.12 [kg m^{-3}]		Caudal fan 1.29 [kg m^{-3}]			
Dielectric properties (at 27.12 MHz), thermal conductivity and specific heat												
	Dielectric loss factor [−]			Dielectric constant [−]			Thermal conductivity [W m^{-1} K^{-1}]		Specific heat [kJ kg^{-1} K^{-1}]			
Temperature	Caudal fan	Cephalon	Tail	Caudal fan	Cephalon	Tail	Caudal fan	Cephalon	Tail	Caudal fan	Cephalon	Tail
−20	4.50	9.91	12.86	8.23	13.97	13.36	0.091	0.827	0.592	1.74	2.81	3.10
−15	10.88	37.33	27.43	12.61	28.95	19.21	0.101	0.893	0.634	2.71	3.70	3.95
−10	23.93	205.75	51.13	17.26	34.67	26.30	0.106	1.03	0.881	4.10	6.08	6.15
−5	28.65	232.36	120.28	18.04	52.34	48.52	0.122	1.25	1.304	4.18	14.06	13.25
0	40.13	328.25	312.63	19.97	98.80	96.36	0.083	1.269	1.178	2.31	15.21	37.89
5	46.98	366.03	350.81	22.52	93.19	97.27	0.083	0.477	0.459	2.24	3.49	3.81
10	68.61	419.71	387.62	25.77	91.89	98.04	0.089	0.457	0.433	2.10	3.33	3.76
15	92.97	470.55	426.43	30.79	96.01	98.79	0.094	0.453	0.464	2.12	3.22	3.70
20	115.51	527.68	486.35	34.72	96.32	100.11	0.102	0.459	0.465	2.14	3.14	3.59
25	125.61	524.76	498.76	36.11	96.75	100.36	0.105	0.467	0.469	2.18	3.16	3.50
30	131.12	554.50	543.74	34.68	100.09	101.48	0.109	0.472	0.472	2.23	4.25	3.49

(LSCI: Loosely stacked crushed ice; CCI: Compacted crushed ice; IB: Ice block).

Table 3
Dielectric and thermophysical properties of ice used in computer simulation.

	Temperature [°C]	Dielectric loss factor [−]	Dielectric constant [−]	Thermal conductivity [W m^{-1} K^{-1}]	Specific heat [kJ kg^{-1} K^{-1}]	Density [kg m^{-3}]
LSCI	0	18.31	0.037	0.78	2062.30	351.01
CCI	0	34.00	0.080	1.25	2062.30	514.82
IB	−20	3.48	0.38	2.39	1940.76	920.00
	−15	3.24	0.26	2.34	1971.15	
	−10	3.01	0.11	2.29	2001.53	
	−5	94.22	0.23	2.25	2031.92	
	0	92.67	0.25	2.22	2062.30	

(LSCI: Loosely stacked crushed ice; CCI: Compacted crushed ice; IB: Ice block).

The volumetric average temperature with standard deviation, the maximum and minimum temperature of all 18 shrimps were directly obtained from the simulation results. The computer-simulated average temperature, *TUI* and the difference between the maximum and minimum temperature of shrimps were used to evaluate the tempering uniformity.

2.6. Model validation

A 12 kW, 50-Ω, parallel-plate RF heating system (Labotron 12, SAIREM Decines Charpeu, France) was utilized for shrimps tempering experiments. The upper plate of the RF heater was made with aluminum with a thickness of 1 cm, which received the generated high voltage from a solid-state generator. The bottom plate was grounded with the main body of the machine. Three bags of frozen shrimps were brought out of the freezer, shrimps were removed from bags and placed in a polypropylene container (28.5 × 19 × 8 cm^3) in 3 layers. Each layer of shrimps was separated with a thin layer of polypropylene film.

Based on a previous study (Koray Palazoğlu and Miran, 2017) and the dielectric properties balancing theory (Jiao et al., 2014), we proposed using an ice block (IB, $\varphi = 0$) as ideal surrounding medium for frozen shrimps and compare with crushed ice in two different porosities. The aim is to study the influence of ice porosity to tempering uniformity of stacked frozen shrimps. Thus, crushed ice was produced and poured into the container with loaded shrimps in two different ways. For loosely stacked crushed ice (LSCI), crushed ice was poured into the container without any mechanical force until fully stuffed in the container. For compacted crushed ice (CCI), crushed ice in the container was pressed by hand with a constant force until all pre-weighted crushed ice was stuffed into the container. The uniformity of ice porosity in both modes was maintained by using a predetermined quantity of ice based on preliminary weight measurements, and the ice volume was controlled to match the container's volume. For ice block mode, three layers of shrimp were put into a container, then filled water into the container until covered three layers of shrimp, the container with water and shrimps were frozen together until the temperature of both reached −20 °C in experiment. The estimation of porosities was explained in *section 2.3.3*.

According to preliminary experiments, an input power of 300 W with an electrode gap of 13 cm was selected as RF heating condition in this current study. Shrimps with and without ice surrounding in containers were individually placed at the center of the bottom electrode of the RF heater ready for tempering experiment. A fiber optic sensor (Heqiguangdian, Xi'an, China) was inserted into the center of one shrimp sample on the second layer for monitoring the temperature-time history. Tempering experiment was stopped when the average temperature of the shrimp reached around −2 °C to obtain a reasonable tempering time for all treatments. From temperature history, 900 s was selected for all RF tempering treatments both with and without ice for reasonable comparison. When reaching the target tempering time, crushed ice was removed immediately, and each layer of shrimps was taken out of the container together and quickly placed under the infrared camera (FLIR A655sc, Wilsonville, USA). The upper surface temperature distribution of all 3 layers of shrimps was photographed. The photographing process was not conducted for shrimps surrounded by IB since previous experiments (Zhang et al., 2021b) showed ice block barely melted when the temperature of shrimps reached 0 °C in RF tempering. This makes the shrimp temperature profile difficult to be obtained and analyzed. In addition, to validate the model, the mean absolute percentage error (MAPE) in (%) was used to compare the center temperature differences of three-layer shrimps between the simulated results and experimental data to validate the simulation model.

$$MAPE = \frac{1}{n}\sum_{i=1}^{n}\left|\frac{(\widehat{y}_i - y_i)}{y_i}\right| \quad (15)$$

where n is number of temperature points, $\widehat{y}_i$ is the simulated temperature value (°C), y_i is experimental temperature value (°C).

3. Results and discussion

3.1. Dielectric and thermophysical properties of shrimps

The dielectric and thermophysical of cephalon, tail and caudal fan are shown in Fig. 3. The thermal energy in shrimp converted from RF electromagnetic is mainly influenced by dielectric properties, including dielectric constant (ε') and dielectric loss factor (ε'') (Dong et al., 2021). The ε' describes the ability of the product to store electromagnetic energy, and the ε'' describes the ability of thermal energy conversion from electromagnetic energy in product (Llave et al., 2014). The dielectric properties of the three parts of shrimp at −20 to 30 °C and 27.12 MHz are shown in Fig. 3 (a, b). The ε' and ε'' of the tail and cephalon of shrimp slightly increased in the temperature range of −20 to −5 °C due to the limited amount of mobile water in frozen shrimp. This result is similar to that reported by Farag et al. (2008). A significant increase in electric properties was observed in the temperature range of −5 to 0 °C. This is because within this temperature range, the ice crystals in shrimp tail and cephalon start to exhibit a phase change, which allows the system absorbing more RF energy to balance the inter-molecular attractions of the sample (Llave et al., 2014). Several studies also reported that the dielectric properties of frozen food products increased significantly during phase transition (Farag et al., 2008; Llave et al., 2014).

As shown in Fig. 3 (c), the specific heat of three parts of shrimp first increased slowly at temperature range of −20 ~ −10 °C, then raised rapidly during −10 ~ −2 °C and reach the peak. The specific heat was 44.36, 38.72, and 4.36 kJ kg^{-1} K^{-1} for tail meat, cephalon, and caudal fan, respectively. The specific heat of caudal fan exhibited the slight variation during −20~30 °C, which may be due to the low water content in shrimp caudal fan. Results indicated the water content had a significant effect on apparent specific heat of three parts in shrimp (Chen et al., 2023).

The thermal conductivity of three parts of shrimp were shown in Fig. 3 (d). The changing trend of thermal conductivity of cephalon and caudal fan was similar at the temperature range of −25~30 °C. The highest value (1.39 W m^{-1} K^{-1}) was found in tail meat at −3 °C. However, it was observed that the thermal conductivity of shrimp caudal fan remained almost constant at 0.1 W m^{-1} K^{-1} with increasing temperature due to limited water content.

The cephalon of shrimp had the highest moisture content (87.4%), followed by the shrimp tail (79.2%), and the caudal fan had the lowest moisture content (43.2%), which was the main reason for the higher dielectric loss factor of cephalon and tail than that of caudal fan. The composition of caudal fan was with limited water content and a main composition of calcium, which indicated that the dielectric properties of caudal fan was insignificantly affected by temperature. Fan et al. (2021) also reported that the moisture content of different sections of crayfish was positively correlated with its dielectric properties.

3.2. Model validation

The simulated and experimental results of shrimps at the center of middle layer are compared in Fig. 4 for model validation. All the temperatures increased as tempering time increases both with and without ice surrounding, but the heating rate increased as the ice porosity decreased. The heating trends of samples with different ice surrounding

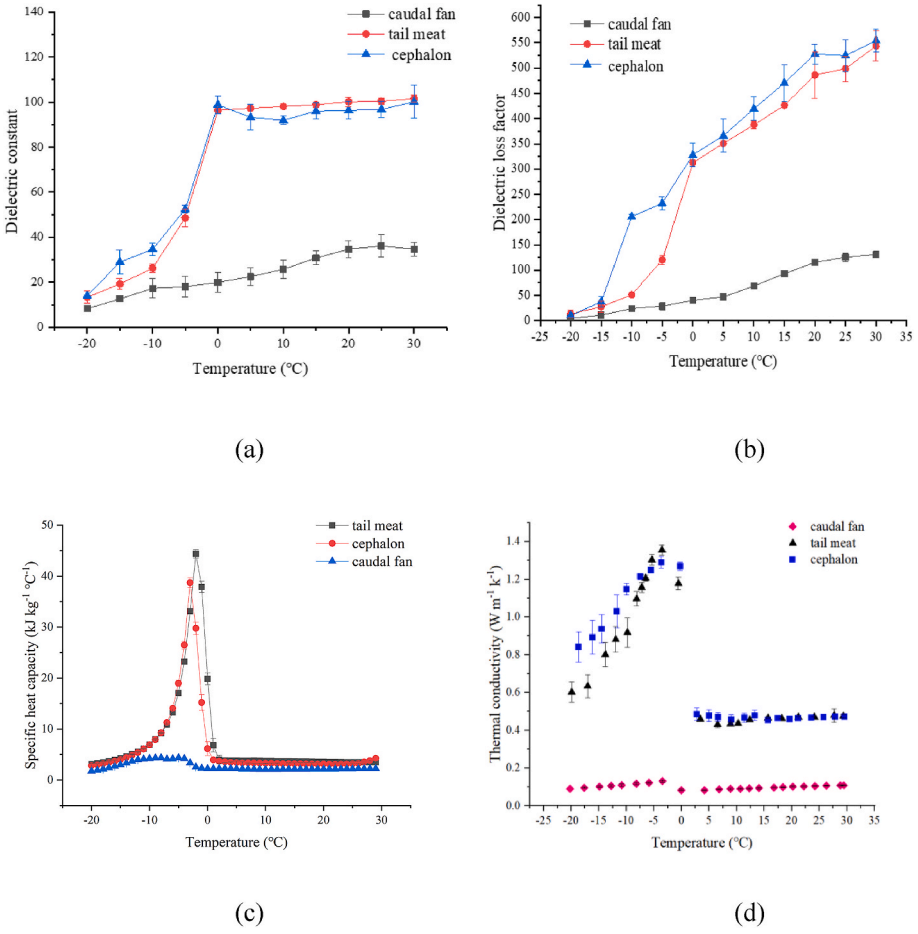

Fig. 3. The dielectric properties (at 27.12 MHz) and thermal properties of cephalon, tail meat, and caudal fan of shrimp within the temperature range of −20~30 °C: (a) dielectric constant ε', (b) dielectric loss factor ε'', (c) specific heating capacity, and (d) thermal conductivity.

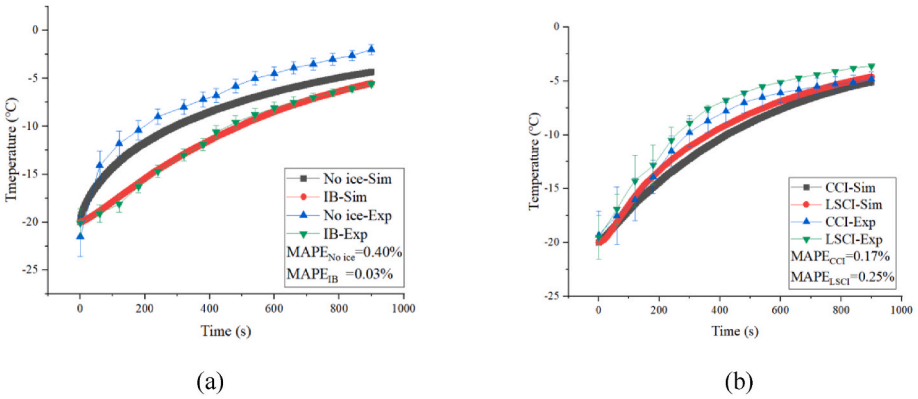

Fig. 4. Comparison of experimental and computer simulation results of RF tempering shrimps at the center of middle layer with different ice surrounding methods: (a) IB and no-ice mode; (b) CCI and LSCI mode (LSCI: Loosely stacked crushed ice; CCI: Compacted crushed ice; IB: Ice block; MAPE: Mean absolute percentage error).

methods was consistent with the corresponding experimental results. Both the simulation and experimental results indicated that the tempering rate of LSCI was higher than that of CCI. The MAPE values for CCI, LSCI, IB and no-ice model were 0.17%, 0.25%, 0.03% and 0.40%, respectively. A lower MAPE indicates a higher prediction accuracy of the model. It worth noting that the experimental temperatures of CCI and LSCI were higher than those simulated. This difference may be attributed to the uneven distribution of pores in crushed ice due to random size and distribution of the crushed ice particulates. This disparity may lead to variations in the electromagnetic field distribution of shrimp between the experiment and simulation, consequently resulting in differences of temperatures. The difference between simulation and experiment for all treatments could also be attributed to the inaccuracies of measured dielectric and thermophysical properties with temperature variation. The difference between simulation and experiment for all treatments could be attributed to the inaccuracies of measured dielectric and thermophysical properties with temperature variation. Shrimps surrounded with CCI and LSCI at the beginning of the RF heating exhibited the temperature deviation of 2.2 and 2.7 °C, respectively. This may be due to the different degrees of thermal exchange occurred between the sample and surroundings during the arrangement of shrimp and also the influence of the insertion of temperature sensor.

Simulated temperature distributions for the top surfaces of three-layer shrimps were compared with experimental results in Fig. 5. From the simulation results, the TUI value of the 1st layer of shrimps tempered without ice was the highest (0.12), which indicates that the tempering uniformity is the worst. The lowest TUI value (0.026) was observed in the 3rd layer shrimp surrounded with LSCI, which indicated that the optimal RF tempering uniformity in shrimps surrounded with CCI. These results were consistent with the experimental results of temperature distribution. The differences between maximum and minimum temperatures and standard deviation of the temperature on the top surface of shrimp were summarized in Table 4. From the simulated temperature results, the overheated area was observed at the caudal fan of each layer shrimps, and the highest temperature was found in the 1st layer of shrimp without surrounding the crushed ice, which reached 48.8 °C. However, the lowest temperature (−4.6 °C) on the surface of the shrimp tail for RF tempering shrimp without surrounding crushed ice. This was consistent with the experimental results. Experimental results showed that the overheated spots were in the caudal fan of three-layer shrimps tempered without crushed ice, and the highest temperature and the lowest temperature was 29.8 and −1.9 °C, respectively. In experiment, a small amount of ice melting was observed but the porosity variation of ice is not considered in modeling. The reduced porosity may result in more RF energy focusing on shrimp, further resulted in underestimation of the shrimp temperature. The overestimation of the maximum temperature was possibly because the sample edges were relatively thin, and those portions depicted in simulation were relatively sharp which caused strong energy focus in simulation. But in experiment, although the temperature thin edges were high right after RF heating, the temperature drop was also fast when transferring to temperature capture, which resulted in an overestimation of simulation (Fan et al., 2021). Higher temperature may cause significant temperature drop due to the low environmental temperature during measurement. Furthermore, the interpolation of dielectric and thermophysical properties with temperature variation used in computer simulation might also cause inaccuracy of prediction.

The temperature distribution on the surface of shrimp was significantly improved by surrounding with crushed ice. The porosity of LSCI and CCI was 0.62 and 0.44, respectively, and the temperature of caudal fan in shrimp surrounded by LSCI was higher than that in shrimp surrounded by CCI. The CCI as a medium for RF tempering improved the heating uniformity most significantly, reducing the difference between the maximum and the minimum temperatures on the surface of shrimp from 53.4 to 7.8 °C. No overheated spot was observed on the surface of the shrimp and a uniformity temperature distribution was found in each layer of shrimps. It was found that the average temperature of the 2nd layer shrimps was the lowest comparing to the other two layers in all simulated results, with an average temperature of −6.9 °C and −6.6 °C when surrounded by LSCI and CCI, respectively. Similarly, literature shows the lowest temperature was also found in the 3rd layer of stacked tilapia fillets subjected into RF tempering (Zhang et al., 2021a). The highest temperature (13.6 °C) of shrimp surrounded by LSCI was found at the caudal fan in the 1st layer, which was consistent with the experimental result that the highest temperature (−2.2 °C) was observed in the same area of shrimp. Thus, the developed model could effectively predict the temperature distribution of shrimp in layers in RF tempering.

3.3. *Effects of crushed ice porosity on temperature uniformity of shrimps*

The simulated temperatures on the surface of the 1st layer of shrimps tempered with different porosities of crushed ice were shown in Fig. 6. The highest temperature was found in caudal fan of shrimp without any surrounding medium. The caudal fan of shrimp was the thinnest part of shrimp, which easily absorbed electromagnetic energy. Both of cephalon and tail showed a uniform temperature distribution, which might be due to the similar dielectric properties and thickness. Therefore, the geometry of shrimp had a great influence on the temperature distribution relative to the composition of shrimp for RF tempering. No localized heating was observed in caudal fan of shrimps surrounded by crushed ice. The temperature distribution uniformity of the sample increased with decreased ice porosity, and the most uniform temperature was found in sample surrounded by CCI. Li et al. (2021) also reported that a more uniform temperature of beef was achieved for beef tempered in RF due to the surrounding medium isolates the air around the sample. Crushed ice as a surrounding medium with a low temperature was

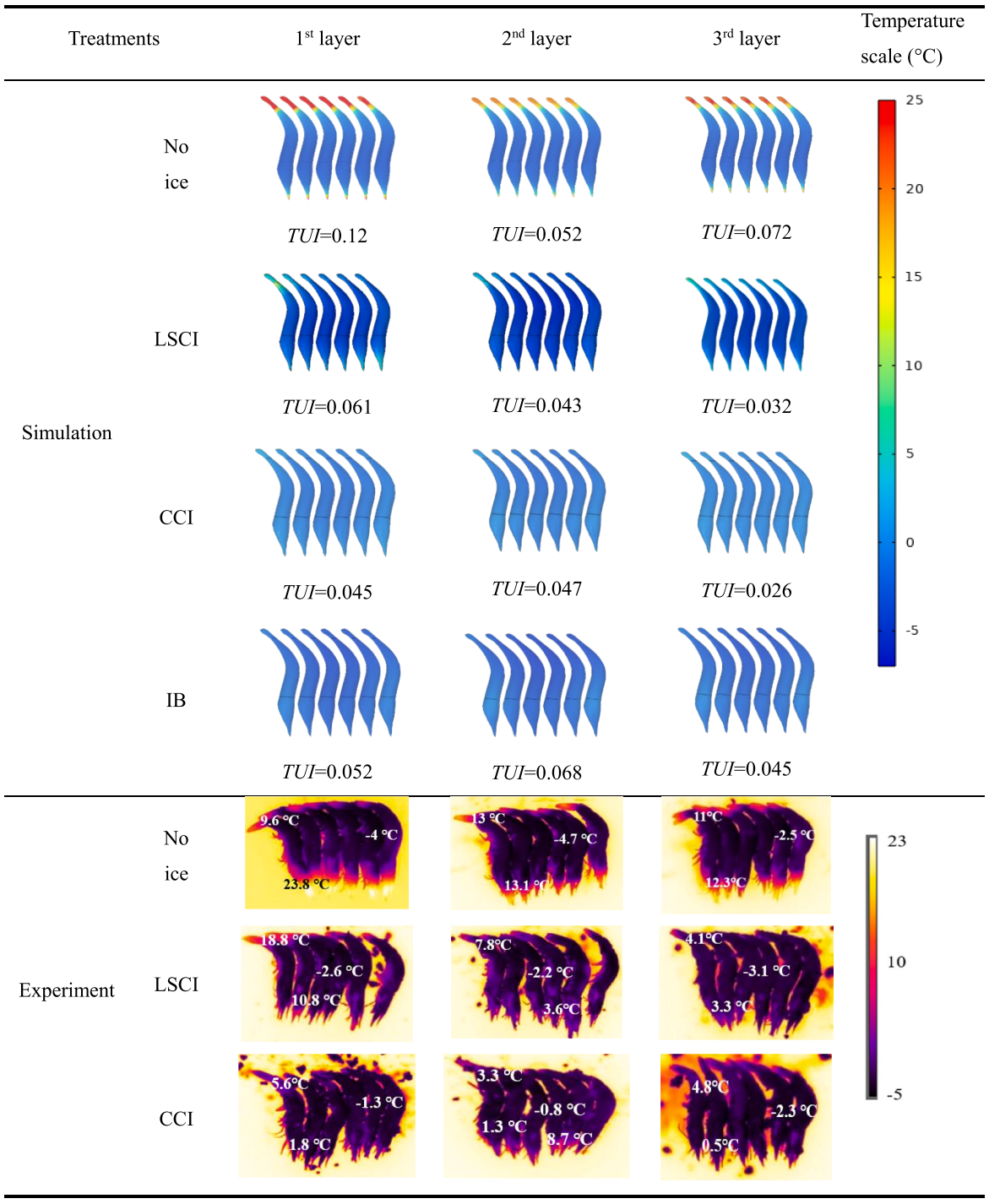

Fig. 5. Temperature distribution of three layers of shrimp without surrounding medium and surrounded by LSCI and CCI for 900 s RF tempering treatment from both experiment and computer simulation. (LSCI: Loosely stacked crushed ice; CCI: Compacted crushed ice; IB: Ice block).

Table 4
Simulated and experimental average temperature of three-layer shrimps surrounded by crushed ice with different porosities after 900 s RF tempering.

Temperature (°C)	No surrounding		LSCI		CCI	
	Simulation	Experiment	Simulation	Experiment	Simulation	Experiment
Average	−1.0	1.7	−4.2	0.93	−4.3	1.4
Standard deviation	–	3.4	–	1.6	–	1.1
Maximum	48.8	29.8	13.6	18.8	1.2	8.7
Minimum	−4.6	−1.9	−6.9	−2.2	−6.6	−0.8
TUI	0.069	–	0.047	–	0.045	–

(*TUI*: Temperature uniformity index; N/A: No surrounding medium; LSCI: Loosely stacked crushed ice; CCI: Compacted crushed ice).

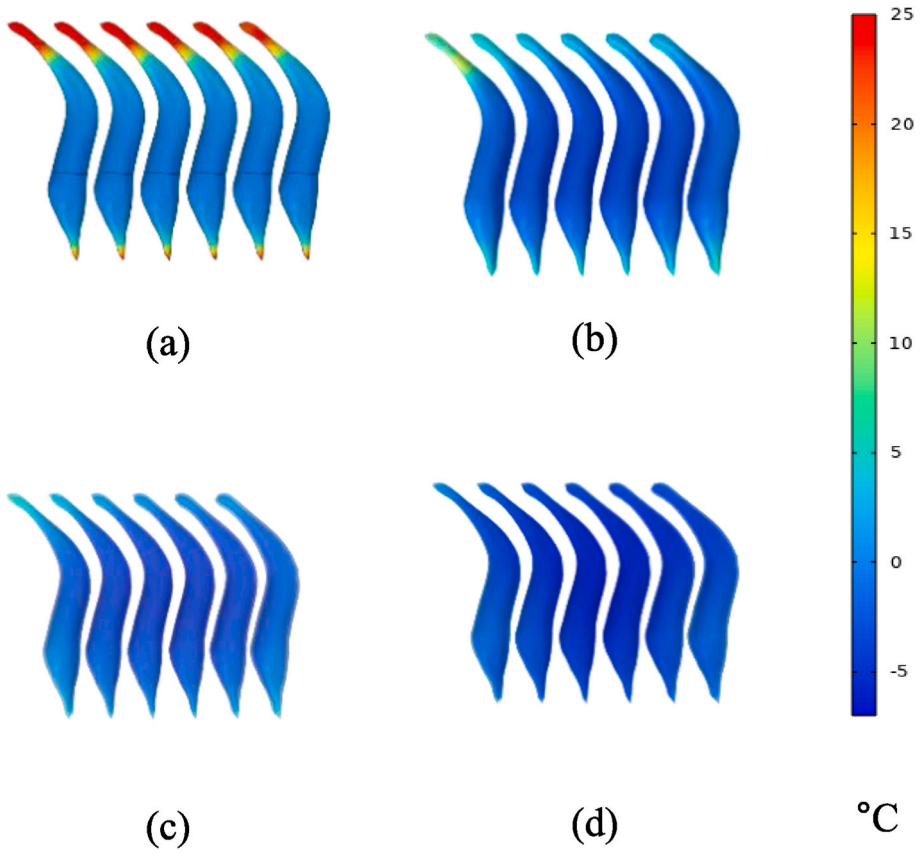

Fig. 6. Temperature distribution of the 1st layer of shrimps without ice (a), and surrounded by LSCI (b), CCI (c) and IB (d) after RF tempering. (LSCI: Loosely stacked crushed ice; CCI: Compacted crushed ice; IB: Ice block).

effective in reducing the edge overheating effect by absorbing excessive heat at the edges and corners of sample (Llave and Erdogdu, 2022). Furthermore, the difference in dielectric constant between the sample and ambient air decreased with increasing the porosity of crushed ice, and evenly distributed electromagnetic field was formed since the interface between the two materials tend to attract less energy and result in uniform temperature (Zhang et al., 2021b).

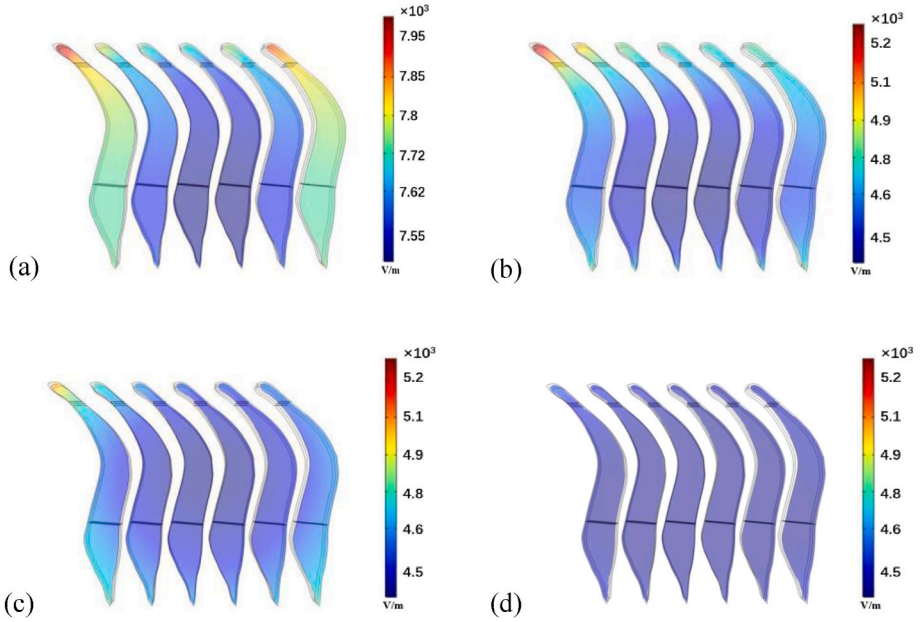

Fig. 7. Simulated electric field intensities of the 1st layer of shrimps without ice (a), and surrounded by LSCI (b), CCI (c) and the IB (d) after RF tempering. (LSCI: Loosely stacked crushed ice; CCI: Compacted crushed ice; IB: Ice block).

3.4. Effects of crushed ice porosity on electric field intensity

The simulated electric field intensities of the 1st layer of shrimp without crushed ice and surrounded with different porosities of crushed ice were shown in Fig. 7. The maximum and the minimum electric field intensities of samples surrounded by various porosities of crushed ice were listed in Table 5. When the samples were tempered without surrounding crushed ice, the caudal fan of shrimp at the edge in the 1st layer had a higher electric intensity (7.97×10^3 V m^{-1}). This was attributed to the electric fields from other directions adding up, leading to a higher field intensity at the corners and edges of sample. Results were consistent with literature that edge heating existed in samples with various shapes, e.g. peanut butter in cylindrical jar (Jiao et al., 2015), frozen beef with irregular shapes (Li et al., 2021), and tuna blocks (Llave et al., 2015). Comparatively, when shrimps were surrounded with crushed ice in RF tempering, the electric field intensity at the edge and thinner area of the sample decreased significantly. The electric field intensities of shrimps surrounded with LSCI, CCI and IB were 5.46×10^3, 5.15×10^4, and 4.37×10^4 V m^{-1}, respectively. The difference between the maximum and minimum electric field intensity of sample surrounded by LSCI, CCI, and IB were 540, 460, and 220 V m^{-1}, respectively. This indicated that the electric field distribution was improved by decreasing the porosity of crushed ice, and the most uniform distribution of the electric field was found in shrimps surrounded with IB, followed by the sample surrounded by CCI and LSCI. The reason was that the dielectric properties of the crushed ice were similar to that of frozen shrimp, which reduced the electric field intensity in sample and thus improved the electric field distribution uniformity. The dielectric constant of crushed ice increased with the decrease of porosity, the ε' of ice with the porosity of 0.62 (CCI), 0.44 (LSCI), and 0 (IB) were 18.31, 34.00, and 92.67 respectively. This indicated an increase in the capacity to store electrical energy in the crushed ice with decreasing the porosity, and thus the strength of the electric field in the shrimps decreased as the porosity of the crushed ice decreased at the same treatment condition.

4. Conclusion

In this study, we evaluated RF tempering effects for three layers of shrimp surrounded by different porosities of ice and with no ice with both experimental and computer simulation methods and analyzed the temperature uniformity and electric field intensity. By taking the composition and geometry of each section of the shrimp into consideration, the computer modeling provides a relatively accurate prediction of the temperature distribution and assist analysis of surrounding medium effects. Crushed ice, as a surrounding medium, can effectively improve the uniformity of electric field intensity distribution and temperature distribution of shrimp after RF tempering. The temperature distribution of shrimp samples was improved by reducing the porosity of crushed ice, and the most uniform temperature was obtained in sample surrounded by compacted crushed ice with a porosity of 0.44, which was consistent with the results of electric field intensity. The proposed method not only enhances the uniformity of shrimp tempering but also simplifies the process of removing shrimp from the crushed ice for subsequent processing.

This research offers a cost-effective and convenient solution for enhancing the radio frequency (RF) tempering uniformity of irregularly shaped food. It demonstrates that RF tempering of shrimp surrounded by compacted crushed ice is an optimal choice for industrial processing. It's important to note that the study did not consider the impact of ice melting on the tempering uniformity of shrimp due to the short tempering time. However, for longer treatment duration, it might be necessary to account for ice melting in order to make more accurate predictions.

Table 5
The maximum and minimum of electric field intensities of the 1st layer of shrimps without ice, and surrounded by LSCI, CCI and IB after RF tempering. (LSCI: Loosely stacked crushed ice; CCI: Compacted crushed ice; IB: Ice block).

Electric field intensity ($\times 10^3$ V m^{-1})	No surrounding	LSCI	CCI	IB
Maximum	7.97	5.46	5.15	4.37
Minimum	7.47	4.92	4.69	4.15

CRediT authorship contribution statement

Yajin Zhang: Writing – original draft, Data curation, Formal analysis, Methodology. **Xiangqing Chen:** Methodology, Validation, Data curation. **Yu Liu:** Methodology, Validation. **Feng Li:** Methodology, Supervision. **Juming Tang:** Supervision. **Hu Shi:** Supervision. **Yang Jiao:** Methodology, Resources, Supervision, Writing – review & editing.

Declaration of competing interest

None

Data availability

I have shared my data at the Attach File step

Acknowledgments

The author acknowledges China National Science Foundation, China (31801613) for its financial support to this research.

References

Birla, S.L., Wang, S., Tang, J., 2008. Computer simulation of radio frequency heating of model fruit immersed in water. J. Food Eng. 84 (2), 270–280.
Cai, L., Zhang, W., Cao, A., Cao, M., Li, J., 2019. Effects of ultrasonics combined with far infrared or microwave thawing on protein denaturation and moisture migration of *Sciaenops ocellatus* (red drum). Ultrason. Sonochem. 55, 96–104.
Chen, X., Li, F., Tang, J., Shi, H., Xie, J., Jiao, Y., 2023. Temperature uniformity of frozen pork with various combinations of fat and lean portions tempered in radio frequency. J. Food Eng. 344, 111396.
Chen, Y., He, J., Li, F., Tang, J., Jiao, Y., 2021. Model food development for tuna (*Thunnus Obesus*) in radio frequency and microwave tempering using grass carp mince. J. Food Eng. 292, 110267.
Chen, Y., Llave, Y., Jiao, Y., Okazaki, E., Sakai, N., Fukuoka, M., 2022. Ohmic tempering using a high frequency ohmic heating and model food of minced tuna based on Allaska pollock surimi – evaluation of electrical conductivities. Innovat. Food Sci. Emerg. Technol. 76, 102940.
Dong, J., Kou, X., Liu, L., Hou, L., Li, R., Wang, S., 2021. Effect of water, fat, and salt contents on heating uniformity and color of ground beef subjected to radio frequency thawing process. Innovat. Food Sci. Emerg. Technol. 68, 102604.
Fan, H., Huang, J., Zhao, J., Yan, B., Ma, S., Zhou, W., Zhang, H., Fan, D., 2021. Electromagnetic properties of crayfish and its responses of temperature and moisture under microwave field. J. Food Eng. 86 (4), 1306–1321.
Farag, K.W., Lyng, J.G., Morgan, D.J., Cronin, D.A., 2008. Dielectric and thermophysical properties of different beef meat blends over a temperature range of -18 to +10 °C. Meat Sci. 79 (4), 740–747.
Guan, X., Wang, Z., Xu, J., Lin, B., Li, R., Wang, S., 2022. Computer Simulation Analyses to Improve Radio Frequency Heating Uniformity for Watermelon Seeds by Inserting Horizontal Aluminum and Polypropylene (PP) Plates in a Rectangular PP Container, vol. 81. Innovative Food Science & Emerging Technologies.
Guo, Z., Ge, X., Yang, L., Ma, G., Ma, J., Yu, Q.L., Han, L., 2021. Ultrasound-assisted thawing of frozen white yak meat: effects on thawing rate, meat quality, nutrients, and microstructure. Ultrason. Sonochem. 70, 105345.
Huang, Z., Datta, A.K., Wang, S., 2018. Modeling radio frequency heating of granular foods: individual particle vs. effective property approach. J. Food Eng. 234, 24–40.
Jiao, S., Deng, Y., Zhong, Y., Wang, D., Zhao, Y., 2015. Investigation of radio frequency heating uniformity of wheat kernels by using the developed computer simulation model. Food Res. Int. 71, 41–49.
Jiao, Y., Tang, J., Wang, S., 2014. A new Strategy to improve heating uniformity of low moisture foods in radio frequency treatment for pathogen control. J. Food Eng. 141, 128–138.
Jiao, Y., Shi, H., Tang, J., Li, F., Wang, S., 2015. Improvement of radio frequency (RF) heating uniformity on low moisture foods with Polyetherimide (PEI) blocks. Food Res. Int. 74, 106–114.
Koray Palazoğlu, T., Miran, W., 2017. Experimental comparison of microwave and radio frequency tempering of frozen block of shrimp. Innovat. Food Sci. Emerg. Technol. 41, 292–300.

Li, F., Zhu, Y., Li, S., Wang, P., Zhang, R., Tang, J., Koral, T., Jiao, Y., 2021. A strategy for improving the uniformity of radio frequency tempering for frozen beef with cuboid and step shapes. Food Control 123 (14), 107719.
Li, Y., Lei, Y., Tan, Y., Zhang, J., Hong, H., Luo, Y., 2022. Efficacy of freeze-chilled storage combined with tea polyphenol for controlling melanosis, quality deterioration, and spoilage bacterial growth of Pacific white shrimp (*Litopenaeus vannamei*). Food Chem. 370, 130924.
Li, Y., Li, F., Tang, J., Zhang, R., Wang, Y., Koral, T., Jiao, Y., 2018. Radio frequency tempering uniformity investigation of frozen beef with various shapes and sizes. Innovat. Food Sci. Emerg. Technol. 48, 42–55.
Liu, L., Llave, Y., Jin, Y., Zheng, D.-y., Fukuoka, M., Sakai, N., 2017. Electrical conductivity and ohmic thawing of frozen tuna at high frequencies. J. Food Eng. 197, 68–77.
Liu, Y., Tang, J., Mao, Z., 2009. Analysis of bread dielectric properties using mixture equations. J. Food Eng. 93 (1), 72–79.
Liu, Y., Tong, T., Han, R., Zhang, Y., Li, F., Shi, H., Jiao, Y., 2023. Effect of different arrangements of globe particles on radio frequency heating uniformity: using black pepper as an example. LWT–Food Sci. Technol. 174.
Llave, Y., Erdogdu, F., 2022. Radio frequency processing and recent advances on thawing and tempering of frozen food products. Crit. Rev. Food Sci. Nutr. 62 (3), 598–618.
Llave, Y., Liu, S., Fukuoka, M., Sakai, N., 2015. Computer simulation of radiofrequency defrosting of frozen foods. J. Food Eng. 152, 32–42.
Llave, Y., Terada, Y., Fukuoka, M., Sakai, N., 2014. Dielectric properties of frozen tuna and analysis of defrosting using a radio-frequency system at low frequencies. J. Food Eng. 139, 1–9.
Marra, F., Lyng, J., Romano, V., McKenna, B., 2007. Radio-frequency heating of foodstuff: solution and validation of a mathematical model. J. Food Eng. 79 (3), 998–1006.
Miran, W., Palazoglu, T.K., 2023. Simulation and measurement of the effects of surrounding material on the uniformity of radio frequency heating of wheat flour. Biosyst. Eng. 227, 130–146.
Mohos, F., 2010. Principles of Food Engineering[M]. John Wiley & Sons, Ltd.
Singh, R.P., Heldman, D.R., 2001. *Introduction to food engineering*. Gulf Professional Publishing.
Tang, M., Cen, J.W., Lai-Hao, L.I., Yang, X.Q., Wei, Y., Hao, S.X., Huang, H., 2017. Impact of high voltage electric field thawing on the quality of frozen tilapia fillet. Science and Technology of Food Industry 156, 39–44.
Tong, T., Wang, P., Shi, H., Li, F., Jiao, Y., 2022. Radio frequency inactivation of E. coli O157: H7 and Salmonella Typhimurium ATCC 14028 in black pepper (*piper nigrum*) kernels: thermal inactivation kinetic study and quality evaluation. Food Control 132, 108553.
Wang, Z., Li, Q., Jiang, S., Wang, X., Wang, S., Hou, L., 2024. Improving radio frequency heating uniformity in cauliflower by changing density in different zones. Food Bioprod. Process. 143, 1–8.
Watanabe, T., Ando, Y., 2021. Evaluation of heating uniformity and quality attributes during vacuum microwave thawing of frozen apples. LWT–Food Sci. Technol. 150, 111997.
Zhang, Y., Li, S., Jin, S., Li, F., Tang, J., Jiao, Y., 2021a. Radio frequency tempering multiple layers of frozen tilapia fillets: the temperature distribution, energy consumption, and quality. Innovat. Food Sci. Emerg. Technol. 68, 102603.
Zhang, Y., Li, F., Yao, Y., He, J., Tang, J., Jiao, Y., 2021b. Effects of freeze-thaw cycles of Pacific white shrimp (Litopenaeus vannamei) subjected to radio frequency tempering on melanosis and quality. Innovat. Food Sci. Emerg. Technol. 74, 102860.
Zuo, Y., Zhou, B., Wang, S., Hou, L., 2022. Heating uniformity in radio frequency treated walnut kernels with different size and density. Innovat. Food Sci. Emerg. Technol. 75, 102899.